Appendix J—Fault-to-Fault Rupture Probabilities

By Glenn P. Biasi,[1] Tom Parsons,[2] Ray J. Weldon, II,[3] and Timothy E. Dawson[4]

Introduction

In this appendix we discuss methods for assigning and evaluating the probability of multi-fault earthquake rupture. Fault-to-fault rupture refers to how earthquake ruptures negotiate geometrical discontinuities, such as gaps and steps in the fault system. The inclusion of the possibility of fault-to-fault jumps is new compared to the methodology adopted by Uniform California Earthquake Rupture Forecast, version 2 (UCERF2) (Field and others, 2009), in which rupture was constrained to single faults in segments determined a priori. In the Uniform California Earthquake Rupture Forecast, version 3, (UCERF3) Grand Inversion (GI), probabilities of ruptures are derived from a mathematical inversion process (appendix N, this report). In this appendix, fault-to-fault rupture probabilities from three sources are examined—empirical observation, physical models, and Coulomb stress interactions. The results contribute in three ways to UCERF3. First, they contribute to rules for constructing ruptures as inputs to the Grand Inversion. Second, they provide a basis and rationale for an improbability constraint, as a resource for the Grand Inversion. Third, fault-to-fault rupture behavior observed in empirical ruptures and physical models provide independent criteria with which to evaluate GI rupture model outputs.

In UCERF3, faults from the statewide Community Fault Model are discretized into subsections extending to the base of the seismogenic layer in depth and an along-strike length of half that amount (that is, typically 15 and 7.5 kilometers (km), respectively). Slip on each subsection is constant. The level at which faults are discretized means that many smaller-scale details are not included. Missing details such as realistic slip and slip-rate tapering into fault terminations and the presence of minor intermediate faults in stepover regions could present difficulties if dynamic modeling were to be applied to the UCERF3 fault model.

A first step in developing rupture probabilities is to develop a suite of possible ruptures. The procedures for the development of ruptures as inputs to the Grand Inversion are detailed in appendix T (this report). The smallest rupture considered in the Grand Inversion consists of two subsections. Rules for linking additional subsections include that gaps in a rupture on a contiguous fault trace are not allowed, fault-to-fault jumps are limited to be less than 5 km, section-to-section azimuth change must be less than 60 degrees, rupture net azimuth change must be less than 60 degrees, rupture total absolute angle deviation must be less than 560 degrees, the cumulative rake change must be less than 180 degrees, and branches at fault-to-fault points must have a minimum level of Coulomb compatibility. See appendix T (this report) for the complete

[1]University of Nevada, Reno.
[2]U.S. Geological Survey.
[3]University of Oregon.
[4]California Geological Survey.

list and a description of their implementation. Ruptures passing this rule set are considered equally likely as inputs to GI with no further review such as for geologic plausibility. *A priori* weights might in principle be included in the Grand Inversion, but in practice *a priori* weights would have severely complicated GI implementation. In addition, it is the role of the GI to set rupture weights, so to include them as inputs would invite the criticism that some rupture probabilities had been assumed from the outset.

Fault-to-fault jumping has been studied by many researchers. In the first computationally based simulations of multi-fault dynamic earthquake rupture, Harris and others (1991) and Harris and Day (1999), who studied models of parallel vertical strike-slip faults, found that simulated ruptures could jump as much as 5 km across dilational steps, but only half that for compressional steps, and that the jumping distance depended on how close the faults were to failure relative to the stress drop. Others have found compressional steps crossed more readily than dilational steps if the regional stress field is favorably aligned to drive the main faults coming into the step (Lozos and others, 2011). Harris and Day (1999), Oglesby (2005, 2008), and Lozos and others (2011) studied various aspects of jumping dynamics as a function of geometry, separation, and the presence of linking faults. Steep slip gradients at fault ends near steps tend to promote fault-to-fault jumps (Oglesby, 2008). The role of fault bends on rupture dynamics and continuation has been studied by, among others, Harris and others (2002), Aochi and others (2002), Kame and others (2003), Kase and Day (2006), Duan and Oglesby (2006), and Lozos and others (2011). The state of pre-stress also affects fault-to-fault jumping probabilities and rupture propagation at fault bends (Bouchon and Streiff, 1997; Bouchon and others, 1998; Harris and Day, 1999; Harris and others, 2002; Poliakov and others, 2002; Lozos and others, 2011). Unfortunately, the state of pre-stress is an unknown and complicating factor for probabilistic rupture predictions.

Well-mapped surface ruptures can provide an empirical basis for developing fault-to-fault rupture probabilities as a function of separation distance and rupture style, with the assumption that fault geometry observed at the Earth's surface is similar to the geometry at depth. We examine three sets of empirical data. One is the relatively well-known set of strike-slip earthquakes and faults from Wesnousky (2008; referred henceforth as “W08”). We also develop fault-to-fault measures for the reverse and normal mechanism events of W08 and add fault-to-fault data from a new set of earthquakes developed for UCERF3 and described in appendix F (this report).

Empirical Fault-to-Fault Probabilities from Steps in Strike-Slip Faulting

We consider first fault-to-fault jumping probabilities based on an ensemble of well-mapped surface ruptures. Wesnousky (2008) studied 37 surface faulting ruptures, 22 of which were strike-slip events. The strike-slip subset was examined in two ways (fig. J1). In the first way, which may be called, “look inside,” we ask how often do ruptures include one step-over, two step-overs, and so on? In a second approach, “look at ends,” we ask how often do ruptures stop at fault steps and fault ends? For both inquiries steps are counted if the surface trace is discontinuous by 1 km or more. How fault traces continue at depth in the Wesnousky (2008) collection is not considered and, in most cases, not known.

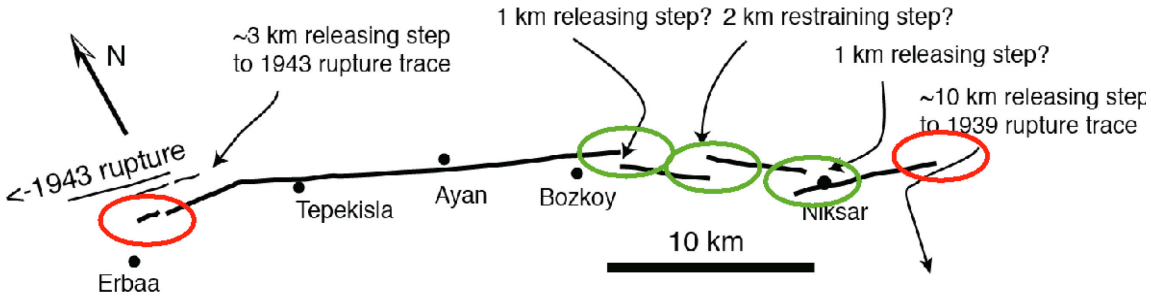

Figure J1. Example surface rupture for the 1942 Erbaa-Niksar, Turkey, event. This event has three interior steps of greater than 1 kilometer (km) in width, and both ends are at discontinuities in the fault trace. The "look inside" approach counts interior steps as indicated by the green ellipses; ends are marked with red ellipses.

Look Inside

The "look inside" counting method yields two relevant observations. First, the number of interior steps shows no clear dependence on rupture length (fig. J2). That is, long ruptures are not more likely to have multiple steps than are short ruptures. We may speculate that longer ruptures occur on larger, more mature faults that have worked out many steps in the process of lengthening and accumulating greater net offset.

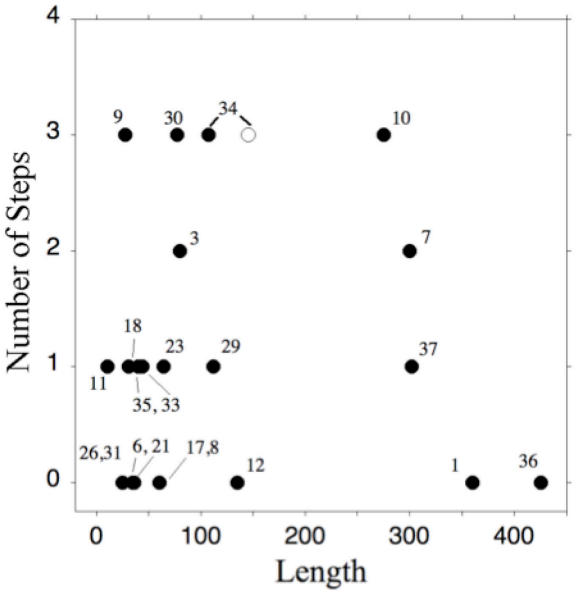

Figure J2. The number of steps in 22 strike-slip ruptures from Wesnousky and Biasi (2011) is plotted versus surface rupture length. Numbers beside points are event numbers in Wesnousky (2008; W08). The open circle on event 34 (1999 Izmit, Turkey) is an alternative length accounting for the underwater part of the event. These data indicate that longer ruptures do not necessarily have more steps.

Second, the data in figure J2 can be recast to suggest the probability that some number of steps will be found in a strike-slip rupture (fig. J3). About half of the ruptures have no steps. About half of the remainder have at least one step. In this dataset no ruptures had more than three steps.

Two probability distributions were fit to these data. The Poisson distribution corresponds to steps occurring at random inside strike-slip ruptures at a mean rate of 1.05 steps per rupture. Physically this distribution may be interpreted as coming from a stress regime with a scale length of the full rupture, and steps are bridged as required if they happen to fall inside that scale length (Wesnousky and Biasi, 2011).

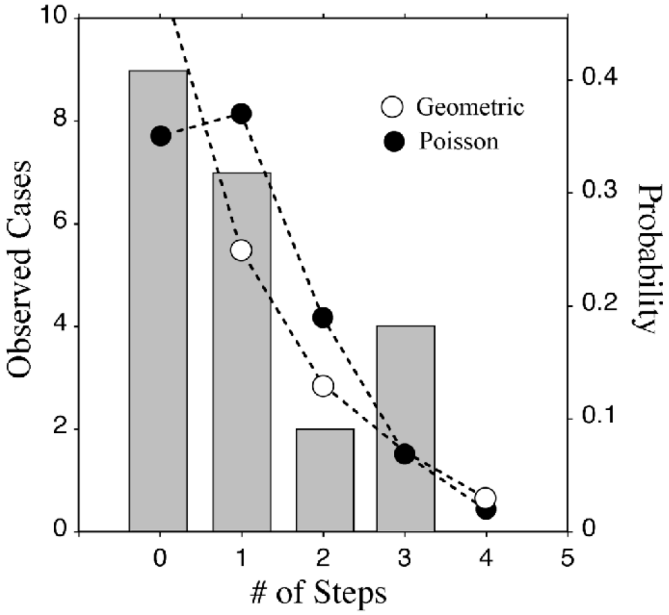

Figure J3. Histogram of numbers of ruptures with a given number of steps. Best-fit Poisson and Geometric probability distributions are also shown. There is no statistical basis to prefer one model over the other. Fitting parameters and their 95 percent ranges are given in table J1. Figure J3 and table J1 are from Wesnousky and Biasi (2011).

Table J1. Probability calculations.
[est., estimate; %, percent]

	Number of steps					Mean est.	95% Range
	0	1	2	3	4		
	Observed fraction and probabilities of occurrence						
Observed fraction	41%	32%	9%	18%	0%		
Geometric probability	0.49	0.25	0.13	0.07	0.03	0.49	0.34–0.63
Poisson probability	0.35	0.37	0.19	0.07	0.02	1.05	0.66–1.57

A geometric probability distribution models fault steps as trials met with some probability of passage p. The number of steps jumped in a randomly chosen rupture is thus $(1-p)^n$. For W08 strike-slip ruptures the probability of jumping a step-over is about 50 percent, corresponding to counting tosses of a fair coin and stopping on the first "tail". For example, jumping 3 or more steps is 0.125 as probable compared to those having zero steps. Physically, the geometric distribution conforms to the intuition that steps require some threshold of conditions to jump, perhaps related to rupture velocity or stress regime, as proposed by Harris and others (1991) and subsequent authors. Although no cases of four or more steps occur in the

W08 strike-slip dataset, both the Poisson and geometric distributions provide some non-zero probability for these cases.

Look at Ends

We may also examine the empirical data for where fault ruptures end. For this substudy, only 21 of the 22 strike-slip events in W08 could be used, the one being excluded because geologic mapping around the ends of the rupture is too poor to categorize the result. For 5 of the 21 ruptures, neither end of the rupture stops at a step or with the end of the mapped fault trace; 9 have one such ending, and 7 have two. Table J2 shows these results as fractions of the total. Also in table J2 are predicted fractions if the probability of jumping a step on the end is 0.5 and steps are reached on both ends. As was the case for the "Look Inside" approach, steps become ends of ruptures with a probability of about 50 percent. About three-quarters of W08 strike-slip ruptures have at least one end at a step-over or fault termination. This ratio may be used to compare with inversion outputs.

Table J2. Fraction of strike-slip ruptures with ends at map-scale geometrical fault discontinuities.

	Neither end	One end	Both ends	At least one end
Number (total=21)	5	9	7	16
Fraction of total	0.24	0.43	0.33	0.76
Predicted at p=0.5	0.25	0.50	0.25	0.75

Empirical data suggest that, to a point, step size may not matter for the probability of jumping (figs. J4 and J5). Figure J4 (Wesnousky, 2006) shows rupture terminations as a function of step size. There are more small steps than larger ones, but for steps as large as approximately 4 km the fraction jumping appears not to be a function of the size of the step (fig. 5). This result is surprising and somewhat at odds with dynamic modeling results and physical considerations, so a larger sample of ground ruptures would be desirable.

We note that for UCERF3 use, a distinction exists in distances available for application of the above empirical criteria. Specifically, the empirical data refer to how far apart the traces of the fault are at the surface. In UCERF3, the available distance measure is of the closest approach between subsections, which need not be at the surface. Thus subsections at a surface step-over may have centrally verging dips and meet at depth and (or) may meet at the surface but diverge at depth. Both cases would be included in inputs to the Grand Inversion. Similar unknowns underlie empirical ratios of jumping. Thus the empirical probabilities of jumping steps based on surface trace separation should reasonably predict probabilities based on the UCERF3 minimum distance of separation.

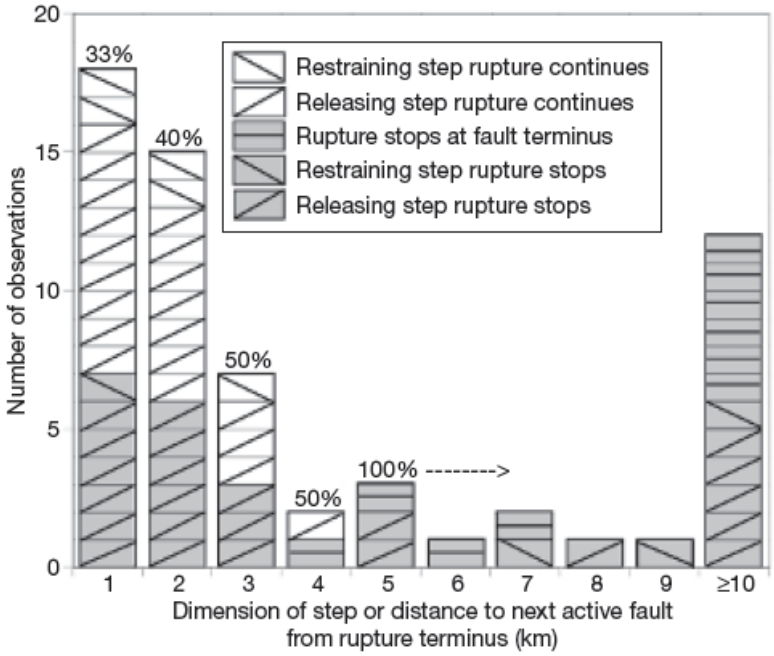

Figure J4. Ruptures jumping and stopping at steps are binned by distance. More small steps are noted than larger ones, but for steps as large as 4 kilometers (km) the fraction through which rupture continues appears not to be a function of the step size.

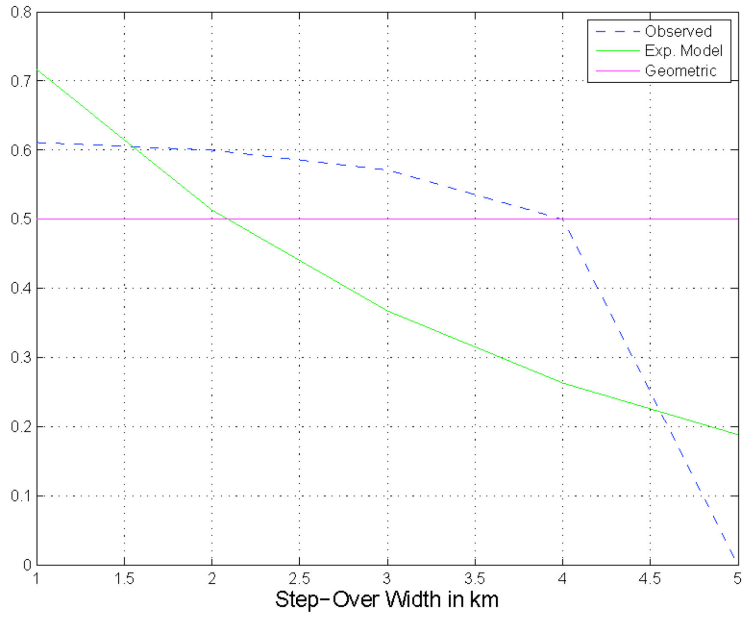

Figure J5. Probability of passing a step of a given width for empirical data in figure J4. The exponential (Exp.) probability model (Shaw and Dieterich, 2007, discussed below) is also shown.

Empirical Fault-to-Fault Probabilities from Branching and Changes in Sense

We may ask how frequently fault-to-fault ruptures occur in the sense of branching at high angles to the main trace or other geometries that are not a simple extension of the primary rupture. We consider events from W08 and the additional event set developed by Biasi, Weldon, and Dawson (appendix F, this report; "BWD12") for rupture length-average displacement regression. For this survey ruptures with small displacements and net lengths less than ~15 km are not used. A change in name alone along strike was not sufficient to count as a fault-to-fault case.

Ruptures from W08 Counted as Fault-to-Fault Cases

- **1896 Rikuu, Japan (reverse):** The Kawafune section is ~12 km distant from the main rupture and opposite in vergence. Two reverse-reverse (r-r) jumps are noted.
- **1915 Pleasant Valley (normal):** Rupture links four sections in an en echelon pattern oblique to the fault strikes. Three normal-normal (n-n) jumps.
- **1954 Fairview Peak (normal):** One n-n jump from the Monte Cristo to the Fairview Fault across a >10 km releasing step at the southern end. Dominant strike-slip on the Fairview Fault changes trend and transitions to two 5 km normal splays, where the rupture ends (ss-n). Other steps to smaller rupture traces are noted.
- **1959 Hegben Lake (normal):** The Red Canyon Fault trace bends toward the Hegben Fault, and would join at 65 degrees from it if the Red Canyon trace continued another kilometer (n-n).
- **1983 Borah Peak (normal):** Main rupture splays 45 degrees continuing as two normal offsets with a 5 km gap in the main trace at the point of the splay (n-n).
- **1988 Tennant Creek (reverse):** Ruptures of opposite vergence are separated by a 6 km step (r-r).
- **1992 Landers (strike slip):** Rupture on the Johnson Valley Fault jumped on a structure 30 degrees oblique it to reach the Homestead Valley Fault (ss-ss). Homestead Valley-Emerson is counted only as a step.
- **2001 Kunlun (strike slip):** West end of rupture follows a SS splay 20 degrees from the main trace (ss-ss)
- **2002 Denali (strike slip):** Rupture started with a thrust mechanism on the Susitna Glacier Fault (r-ss), and followed the Totchunda splay instead of staying on the main trace of the Denali rupture (ss-ss).

The normal and reverse mechanism ruptures of W08 are summarized in table J3. It is clear that the sizes of the steps crossed by normal and reverse mechanism ruptures are much greater than for strike-slip ruptures. Corresponding strike-slip rupture steps and gaps are tabulated in W08 and Wesnousky (2006) and not repeated here.

Table J3. Normal and reverse mechanism events in W08.

[*M*, magnitude; Nsteps, number of steps; N, normal; R, reverse; Nd, no data; -, not applicable; r-r, reverse-reverse; n-n normal; ss-n, strike slip-normal; km, kilometers]

Event	*M*	Style	End	End	Nsteps	Step size (km)	Fault-to-fault jumps and branches[3]
1887 Sonora, Mexico	7.2	N	Nd	Nd	1	2	None
1896 Rikuu, Japan	7.2	R	Fault ends	Open	3	2 8 12	- r-r r-r
1915 Pleasant Valley, Nevada	7.3	N	Fault ends	Fault ends	3	4 4 7	n-n n-n n-n
1945 Mikawa, Japan	6.2	R[1]	Fault ends	Offshore, unknown	0	-	None
1954 Fairview Peak, Nevada	7.0	N to SS	Open	Fault ends at 5 km step	4	2 10 3 1 -	- n-n - - 2 x ss-n[2]
1954 Dixie Valley, Nevada	6.8	N	Open	Open	1	3	None
1959 Hegben Lake, Montana	7.0	N	Fault end, 9 km step	Open	1	5	n-n
1971 San Fernando, California	6.7	R[1]	Unclear	Unclear	1?	1	None
1979 Cadoux, Australia	6.1	R[1]	Unclear	Unclear	-	-	-
1980 El Asnam, Algeria	6.7	R	Unclear	Unclear	0	-	None
1983 Borah Peak, Idaho	6.9	N	Open	Open	1	4	n-n
1986 Marryat, Australia	5.9	R	Unclear	Unclear	0	-	None
1987 Edgecumbe, New Zealand	6.3	N[1]	Open	Faults end	5	2 3 3 1.5 3	-
1988 Tennant Creek, Australia	6.6	R	Unclear	Unclear	1	6	r-r
1999 Chi Chi, Taiwan	7.4	R	Fault ends	Ends at cross fault	0	-	None

[1]Rupture too short or too irregular to include.

[2]Two minor normal splays (~5 km).

Surface Ruptures from Biasi and Others (appendix F, this report) with Fault-to-Fault Jumps

- **1905 Bulnay (strike slip):** The Teregtiin Fault forks at 20 degrees, increasing to 60 degrees, from the main trace south for 70 km, right-lateral strike-slip offset. A second SS rupture, on the Dungen Fault, is 30 km long and joins as an apparent conjugate rupture, at 90 degrees (!). The Dungen Fault is located near where the Tsetserleg trace joins the main Bulnay rupture. The Tsetserleg earthquake occurred 2 weeks before Bulnay and likely influenced this geometry. Both secondary ruptures are consistent with a maximum deviatoric stress direction near N. 30° E. (two strike-slip to strike-slip (ss-ss) jumps).
- **1931 Fuyun (strike slip):** One clear jump, main strike-slip 45 degrees onto a thrust structure ~10 km long (ss-r). Displacement on the thrust is small enough that the main trace displacements continue approximately constantly. One splay of 10 km strike-slip to a strike-slip fault (ss-ss). Both features are secondary and appear to relieve fault-normal stresses (ss-r; ss-ss).
- **1957 Gobi-Altai (strike slip):** Off-main trace ruptures have several meters (m) of displacement. One with ~4 m displacement is 32 km long joins as strike slip at 90 degrees (ss-ss) then hooks 90 degrees to become a thrust at a 40 degree dip; another 70 km long joins the main trace at an angle of 70 degrees as a thrust fault dipping about 49 degrees (ss-r).
- **2008 Wenchuan (thrust):** major duplexing of rupture—72 km long Pengguan trace, 10 km from main trace (r-r). The duplexed rupture is likely to join the main fault at depth. This rupture transitions from reverse-oblique to strike slip from south to north, but not as a fault-to-fault rupture.

The complete list of BWD12 events is in table J4.

Results for the W08 and BWD12 event collections are in table J5. Table J5 shows that fault-to-fault jumping is more likely for normal and reverse faulting events than for strike-slip ruptures. To the extent that they can be compared, W08 and BWD12 event sets yield similar patterns. Less than one in five strike-slip ruptures includes a fault-to-fault jump or significant splay, whereas normal and reverse mechanism events jump or branch at two to three times that rate.

The pattern of more frequent fault-to-fault ruptures in normal and reverse earthquakes than for the strike-slip case may be related to the orientations of principal stresses. For normal faults the greatest principal stress is nominally vertical and the least stress is horizontal. Dilational strain accumulates at the toe of the fault, perhaps with a general strike direction, but at a depth at which it can influence other faults. Reverse and thrust ruptures follow a similar mechanical process except with compressional strains at depth and the least principal stress approximately vertical. Neither principal stress acts to guide the surface trace of the rupture. Thus normal or reverse faults of opposite vergence can rupture in a single event and be mechanically consistent. Examples of both may be found in the W08 event set. Strike-slip ruptures, on the other hand, have both greatest and least principal stresses in the horizontal plane. Active faulting concentrates on vertical planes 30–45 degrees from the direction of the greatest principal stress, and only faults in this orientation can release accumulated strike-slip stresses.

Table J4. Step Widths and Fault Branching for Events in BWD12.

[*M*, magnitude; Nsteps, number of steps; SS, strike slip; R, reverse; Nd, no data; -, not applicable; r-r, reverse-reverse; n-n normal; ss-n, strike slip-normal; deg, degrees; km, kilometers]

Event	*M*	Style	End	End	Nsteps	Step sizes	Branches
1872 Owens Valley, California	7.5	SS	Nd	Nd	Nd	-	Nd
1905 Bulnay, Mongolia	8.4	SS	Nd	Nd	Nd	-	ss->ss ss->ss
1911 Chon Kemin, Kyrgystan	7.7	Rev	Nd	Nd	1[1]	9 km	r->r
1920 Haiyuan, China	8.25	SS	Nd	Nd	4+	>1 km releasing	None
1923 Luohuo, China	7.2	SS	Nd	Nd	Nd	-	Nd
1931 Fuyun, China	7.9	SS	Nd	Nd	Nd	-	ss->r ss->ss[2]
1937 Tuosuo Lake, China	7.5	SS	20 deg change in strike	Open	1	5 km releasing	None
1957 Gobi-Altai, Mongolia	8.1	SS	45 deg trend to thrusting	Trend change into thrusts	4+	-	ss-r ss-ss
1963 Alake Lake, China	7.0	SS	Open	20 deg change in strike	0	-	None
1970 Tonghai, China	7.2	SS	Nd	Nd	3	1.5 km; 1.5 km 1.5 km	None
1973 Luhuo, China	7.4	SS	Nd	Nd	0	-	None
1976 Motagua, Guatemala	7.5	SS	Nd	Nd	0	-	None
1995 Sakhalen, Russia	7.0	SS	Nd	Nd	0	-	None
1997 Manyi, China	7.5	SS	Nd	Nd	Nd	-	Nd
2003 Altai, Mongolia	7.2	SS	Nd	Nd	Nd	-	None
2005 Pakistan	7.6	R	Nd	Nd	1	2 km	None
2008 Wenchuan, China	7.9	R	Nd	Nd	2	-	r-r
2008 El Mayor, Mexico	7.2	SS	Open	Open	0	-	None
2008 Darwin, New Zealand	7.0	SS	Nd	Nd	2	1.5 km; 1.5 km	None

[1]Also a 24 km gap in the surface trace.

[2]Accommodation structures 10 km in length.

The Landers rupture involved several mapped faults almost certainly because the stresses to be relieved were acting obliquely to their traces instead of being favorably released by any of the individual faults (Bouchon and others, 1998). The 1905 Bulnay and 1957 Gobi-Altai ruptures have large secondary ruptures, but they also can be explained by a relatively constant horizontal stress regime. Beside stress field considerations, in strike-slip earthquakes the dynamic forces of

ground rupture act in the direction of rupture propagation, and thus favor linear rupture, whereas dynamic forces in dip-slip earthquakes exert much less influence on adjacent fault sections.

Table J5. Incidence of fault-to-fault rupture by main trace rupture style. Normal and reverse mechanism events have a higher incidence of fault-to-fault rupture.

[W08, Wesnousky (2008); BWD12—Biasi, Weldon, and Dawson (appendix F, this report); F2F, fault-to-fault]

Style	W08 total	Use[1]	F2F	Fraction	BWD12 events	Use[2]	F2F	Fraction	Fraction, combined Set
Normal	7	6	4	0.67	0	-	-	-	0.67
Reverse	8	5	2	0.40	3	3	1	0.33	0.38
SS	22	21	3	0.14	16	13	3	0.23	0.18

[1]Excludes events 11, 13, 19, 20, and 27 from W08 table 1; length too short or mapping insufficient.

[2]Excludes 1872 Owens, 1923 Luohuo, and 1997 Manyi; mapping not sufficient.

Table J6 summarizes the branching described in table J4 by main rupture and branch type. Note that ruptures can have more than one branch or fault-to-fault jump.

Table J6. Fault-to-fault style cases.

[W08, Wesnousky (2008); N, normal; R, reverse; SS, strike slip]

W08	Rupture to:			BDW12	Rupture to:			Joint			
Main	N	R	SS	Main	N	R	SS	Main	N	R	SS
N	6	0	1	N	0	0	0	N	6	0	1
R	0	3	1	R	0	2	0	R	0	5	1
SS	0	0	3	SS	0	2	4	SS	0	2	7

Table J6 makes the point that fault-to-fault jumps and branches tend by a significant margin to stay with the faulting style of the main trace. That is, a strike-slip rupture is much more likely, if it jumps or branches, to continue on another strike-slip structure.

Table J7 summarizes the ratios of fault-to-fault jumps as a function of main fault and alternate fault mechanisms. On average the normal mechanism main faults in this dataset are associated with one jump to another normal mechanism trace. Reverse mechanism ruptures likewise often are associated with a jump to another reverse fault. Ruptures are much less likely to change types, with the most likely, strike-slip to reverse, being observed in about 7 percent of cases.

Table J7. Fault-to-fault jumping incidence by main and alternate fault mechanisms.

[Ratios are computed with table J6 "joint" counts in the numerator and the total number of events (SS_R, SS+N) from table J5 in the denominator and combined in the upper diagonal. On average normal mechanism events are associated with one fault-to-fault jump. N, normal; R, reverse; SS, strike slip]

Fault	Combined event set fault-to-fault rupture ratio		
Main rupture	N	R	SS
Normal	1.0	0	0.03
Reverse		.63	0.07
Strike slip			0.21

Fault-to-Fault Rupture Jumping Probabilities from 2-D Numerical Modeling

Shaw and Dieterich (2007) studied probabilities of fault-to-fault interactions using a two-dimensional (2-D) scalar numerical model consisting of a network of parallel faults. Dynamic fault interactions developed around flaws that were randomly introduced (fig. J6). With shearing of this plate, faults develop. As the faults begin to interact and connect, the probability of linking (a fault-to-fault jump) can be developed as a function of fault separation r (fig. J7). For seismic hazard estimation purposes Shaw and Dieterich (2007) propose a probability of jumping, $p(r) = e^{-r/r0}$, with scale length r_0 ~3 km, based on a fit to the steeply descending portion of the log-probabilities. The choice of r_0 for UCERF3 can be set empirically. A value $r_0 = 1.44$ corresponds to a penalty of 0.5 for a 1 km distance between subsegments, the same as for empirical steps. This value of r_0 leads to an approximately 1 in 30 probability that a step of 5 km might be crossed, which is reasonable considering the Wesnousky (2008) and new strike-slip rupture data.

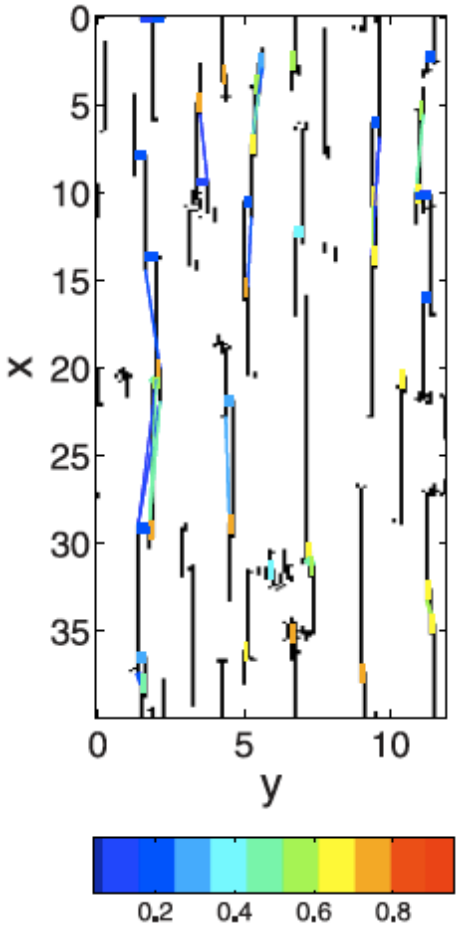

Figure J6. Shaw and Dieterich (2007) model to estimate probabilities of fault-to-fault rupture in a spontaneously evolving strike-slip faulting system. Black lines show faults which have slipped, with the probability that both slip if one slips given by the color bar.

The exponential model has the property of improbability accumulating even for small separation distances. This is perhaps not best suited for use in UCERF3 because subsection

discretization is on the order of 1 km. Where fault subsections might intersect in the real earth, the model could have small gaps because of the discretization that through the exponential model could unintentionally penalize a rupture. The function $p(r) = [1/r^2; 1]$ for (r>1; r<=1) has a very similar roll-off with increasing distance, but would not penalize ruptures with small gaps in them. Heuristically, the $1/r^2$ function can be justified if the rupture front proceeds roughly on a line perpendicular to the direction of rupture propagation; in this case for a rupture to proceed, the volume that must be energized to bridge to the next segment increases with separation as r^2.

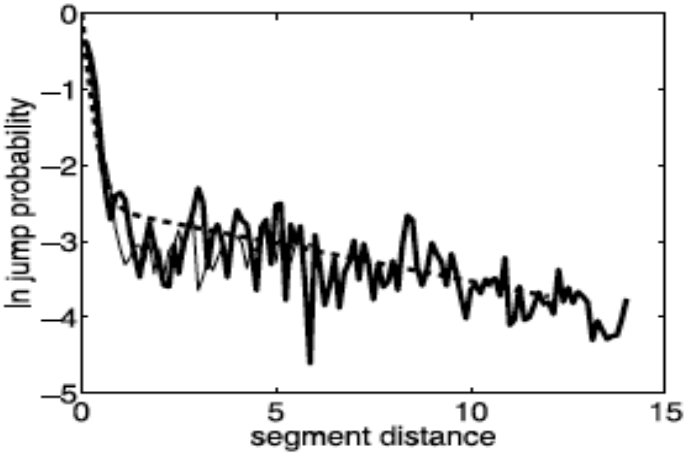

Figure J7. Natural log (ln) of jumping probability as a function of distance between faults. Unit segment distance corresponds to a seismogenic crustal thickness. From Shaw and Dieterich (2007).

Fault-to-Fault Probabilities from Coulomb Interactions

Coulomb stress interaction provides a mathematical method for evaluating the static stress interactions between dislocations in the earth (Reasenberg and Simpson, 1992; King and others, 1994; Parsons and others, 1999; Lin and Stein, 2004; Toda and others, 2011). When applied to consecutive sections in a rupture, the method provides a way that strengths of section-to-section interactions may be characterized. Coulomb stress changes and their ratios are not probabilities per se, but probabilities may be proposed if the ratios of stress interactions are interpreted as averages over multiple ruptures. Dynamic stress transfer is recognized as more efficient at triggering nearby, rupture continuations but is not included in UCERF3 because of the large uncertainties in necessary stress and physical parameters, the need for more detailed fault geometric information, and the very large increase in required computations. Coulomb interactions among fault sections are used in UCERF3 as a Boolean criteria for allowing fault-to-fault jumps but actual probabilities from Coulomb interactions are not. We discuss Coulomb interactions here to capture work done to explore their potential to evaluate the UCERF3 rupture forecast.

The method of estimating Coulomb interactions for UCERF3-style fault subsections is described in Parsons and others (2012), and its implementation for rupture development is described in appendix T (this report). An average measure of interaction is first developed. To do this shear stress change, DS, and change in Coulomb stress, DCCF, are computed for each potentially linked pair of subsections. DCCF includes changes in normal stress, and thus is important for noncoplanar fault segment interactions. The computation assumes a unit

displacement on the first section and projects stress change on the second. An average interaction is required because the calculation is not, in general, symmetric. That is, it does not yield the same stress changes when the second section is treated as the source affecting the first. For example, a fault bend may be either releasing or restraining, depending on rupture direction. The probability $P\Delta CCF_{i,j}$ of branching from the *ith* subsection to the *jth* is the ratio of ΔCCF_j to the sum of ΔCCF over all the *ith* subsection partners. Table J8 shows the top few lines of the Coulomb interaction table. S1 and S1 are section numbers, Δσ is the shear stress change, ΔCCF is the Coulomb interaction (bars), PΔσ is the ratio of Δσ to the sum of Δσ for the section, and PΔCCF is the ratio of ΔCCF to its respective sum. Distance is the minimum separation distance between sections.

Table J8. Section pairs (S1, S2), shear stress change (Δσ), Coulomb interaction (ΔCCF), probability from shear stress change (PΔσ), probability from Coulomb interaction (PΔCCF), and separation distance used for estimating Coulomb interactions among UCERF3 fault subsections.

S1	S2	Δσ	ΔCFF	PΔσ	PΔCFF	Distance (km)
0	1	23.051	23.067	0.779	0.754	0.00
0	1122	0.248	0.471	0.008	0.015	4.53
0	1123	3.620	5.065	0.122	0.166	0.37
0	1124	1.428	0.939	0.048	0.031	0.72
0	1125	1.237	1.043	0.042	0.034	3.18
1	0	23.074	23.09	0.210	0.212	0.00
1	2	85.408	84.657	0.777	0.778	0.00
1	1124	0.734	0.705	0.007	0.006	3.40
1	1125	0.667	0.3	0.006	0.003	3.40
2	1	80.837	80.119	0.310	0.308	0.00
2	3	180.169	180.401	0.690	0.692	0.00
3	2	168.040	168.256	0.960	0.959	0.00
3	4	6.999	7.22	0.040	0.041	0.00
4	3	6.735	6.885	0.098	0.101	0.00
4	5	61.667	61.146	0.902	0.899	0.00
5	4	77.608	76.988	1.000	1.000	0.00

In UCERF3 application, Coulomb interactions were used only in the rupture creation stage, with other criteria, to decide which ruptures could be considered plausible, and therefore be included as input to the GI (appendix T, this report). Coulomb interactions might also be used in model evaluation, to compare Coulomb interaction ratios with rates that fault branches occur in the rupture forecast. Please see the Applications in UCERF3 section at the end of this document for more details about Coulomb modeling.

Empirical Interaction Using Slip Vector Divergence

The definition of each subsection in the fault model includes a slip vector. This vector indicates the long-term sense in which strain is relieved on that section. The degree of consistency from subsection to subsection in a rupture is thus a measure of whether the sections are likely to rupture in the same earthquake. If slip vectors are not parallel, slip together will involve a space problem normally expressed by topographic indicators near the fault. If ruptures are constructed on the basis of section proximity alone, sections can be linked into ruptures that are inconsistent. For example, the Coast Range thrust faults are near in some places to parallel-trending strike-slip faults. However, the slip vectors for the two are substantially inconsistent, as they trend northeast and northwest, respectively. The two faults can coexist without linking if, as is generally thought, the thrust fault relieves fault-normal stress accumulations that build on the strike-slip system. In terms of principal stress directions, the largest principal stress (σ_1) for a N. 45° W. trending right-lateral strike-slip fault would be between N. and N. 15° W. (30–45 degrees clockwise from the fault). For the N. 45° W. striking thrust, σ_1 is directed northeast, 45 to 60 degrees clockwise from σ_1 for the strike-slip case. Lozos and others (2011) find that the orientation of the regional stress field controls rupture favorability more than dynamic or static fault interaction effects.

Consistency of motion in the context of a regional stress field is then a potential screening criteria for multi-fault ruptures allowed as inputs to the GI. Slip vectors more than 65 degrees apart on adjacent sections are sufficiently inconsistent that they can be removed without loss. Based on a northern California rupture sample, this criterion could reduce the number of ruptures input into the GI by about 10 percent.

Slip-vector consistency may also be used as a weighting for ruptures. In outline, section pairs that are parallel and have the same rake have no penalty; pairs with angular discordance are penalized by the likelihood that rupture would pass a change in orientation of that angle. A weighting function is shown in figure J8. Probabilities are approximate, as they average over restraining and releasing bends (for example, Lozos and others, 2011; Kase and Day, 2006) in order to represent the probability in the absence of knowledge of the rupture direction. Separation distance is neglected or may be applied separately. For the complete rupture to occur, all the section pairs must rupture, so the probability of the rupture reflects the accumulated penalties of each pair.

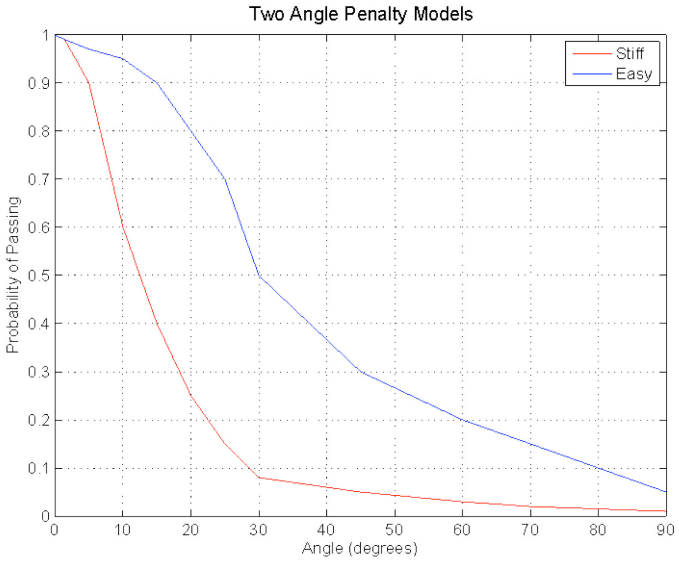

Figure J8. Schematic probabilities of pair-wise rupture propagation given the angle between slip vectors. The red line represents a "stiff" penalty for slip angle changes; the blue line is "easy". Available modeling results (Lozos and others, 2011) generally fall between the two models. If used as an input constraint, the easy model is preferred so that the Grand inversion does most of the final weighting.

The slip vector pair probabilities are roughly based on the probabilities with which rupture continue at changes in trend of different magnitudes. The strong decline in probability at as much as 30 degrees reflects the range beyond which the principal stress direction on the first section would be consistent with motion on the second. The slip vector approach to probabilities is a means of weighting whole ruptures on the basis of their sinuosity and weighting when the rupture direction is not known.

Applications in UCERF3

Distance weighting, Coulomb interactions, angle divergence, and empirical observations were considered for use in UCERF3 in several ways. They are summarized in table J9. Two classes of data were used in the GI, empirical observations suggesting a maximum jumping distance and a Coulomb interaction criteria. These two were applied as Boolean criteria to decide whether a rupture was plausible or not (appendix T, this report). Other uses of distance criteria, Coulomb interactions, and slip compatibility in the GI were considered to reduce the number of input ruptures, but in the end were considered unnecessary. Implementation of improbability constraints within the GI (appendix N, this report) would have introduced significant complexity to the inversion. In addition, it is the role of the GI to set rupture probabilities, so the use of *a priori* probabilities could have the effect of assuming or unduly influencing rupture rates instead of solving for them. The third use of distance criteria, Coulomb interactions, and slip compatibility is to provide an independent probability set with which to evaluate the UCERF3 rupture-rate predictions (table J9, Output Model Evaluation column). The value has not been demonstrated, so the uses described below should be considered prospective tools for a future UCERF.

Table J9. Fault-to-fault approaches and potential applications to UCERF3.
[GI, Grand Inversion; SS, strike slip; N, normal; R, reverse]

	Making input ruptures	Improbability constraints	Output model evaluation
Empirical observations	Inform maximum jumping distance (used in the GI)	Geometric improbability based on number of steps	Comparison with frequency of SS-SS, SS-N, SS-R, N-N, and R-R ruptures in mapped ruptures
Coulomb static stress interactions	Fault-to-fault rupture viability based on minimum strength of interactions (used in the GI)	Down-weight ruptures with unfavorable connections	Compare Coulomb ratios to the earthquake rupture forecast ratios at fault-to-fault "choices"
Slip vector divergence	Remove improbable interactions of opposite sense or at high-angles	Probability based on product of penalties for angle deviations	Compare product angle penalties; include in rupture complexity measures.
Distance measures	Distance-based removal for least probable jumps	Probability from products of penalties based on jump size and number	Compare GI probabilities to predictions; integrate into complexity measures
Rupture complexity	Cut-off based on joint jumping distance and angle divergence penalties	*A priori* probabilities from jumping distance and angle divergence	Compare GI probabilities to independent prediction from complexity.

Direct Application of the Geometric Distribution

In this approach, each rupture is weighted independently on the basis of the distance between subsections. For each pair of subsections where the minimum distance d_{min} between a subsection is more than 1 km from the next nearby, the probability is decreased by a factor of 0.5. Numerically, rupture probabilities will be $(0.5)^{-n}$, for n=0, 1, 2, . . . This applies the Geometric distribution model of Wesnousky and Biasi (2011) without concern for the actual separation between subsections so long as it is greater than 1 km. The rupture probability P_r is:

$$P_r = \prod p_{s,s+1}(d_{min}), \text{ where } p_{s,s+1} = \{ 1 \text{ if } d_{min} < 1 \text{ km; } 0.5 \text{ if } d_{min} >= 1 \},$$

and the product is over all consecutive sections $s,s+1$. This approach could be applied as an improbability constraint in the GI, but has not been applied.

Exponential Distance Penalty

For each adjacent subsection pair in each rupture, calculate a linking function $p(r) = e^{-r/r0}$, with distance $r = d_{min}$, and r_0 as a variable. The probability for each rupture is the product over all adjacent pairs. Note that for r=0, there is no down weighting. The nearest separation distance between subsections sections is used for r. For a value r_0=1.47, the probability increment for a 1-km step would be 0.5, as for (1) above, and a 5-km step would have a probability of roughly 1 in 30.

$$P_r = \prod \exp(-d_{min}/r_0),$$

where the product is over all consecutive section pairs. This approach has not been applied in the GI.

Modified Distance Penalty Distribution

Proceed as with (2) above, but with $P_r = \prod[(1/r^2),\ r>1;\ 1\ otherwise]$. This function matches the empirical step model at r=1 km and decays similar to the exponential model. Among present distance-related probability models, this would be preferred because it is more consistent with the discretization of the UCERF3 model but retains a penalty for increasing separation distance.

Slip-Vector Consistency Weighting

For each adjacent section pair in each rupture, calculate the cosine of the angle θ between slip vectors. Use the angle $cos^{-1}(abs(\theta))$ in figure 8 to obtain the pairwise probability $p_{s,s+1}$. The absolute value corrects for cases where the strike is the same but the dip direction changes. The rupture probability is then:

$$P_r = \prod p_{s,s+1},$$

where the product is over all consecutive section pairs.

The result is probabilities for full ruptures that reflect internal trend changes and that do not depend on (or coarsely average through) rupture direction. Slip-vector direction was considered pre-screen ruptures, but the Coulomb weighting below was preferred because it includes friction and other static effects.

Categorical Weighting Based on Fault Types and Jumping Frequency

Apply table J5 to compare frequency of fault-to-fault involvement by rupture type and table J7 to compare frequencies of change of type in ruptures either as an input global weighting or as a test after inversion. This method has not been implemented.

Coulomb Weighting

Ruptures probabilities might be assigned from the least probable Coulomb link in a rupture or from the average probability over all pairs in the rupture. Pending an improved understanding of the probabilistic basis for whole rupture use of Coulomb factors, Coulomb weighting is used in the GI only at the rupture development phase as a physically based way to assess a rupture's ability to jump a gap

Combined Displacement and Slip-Vector Consistency—Rupture Complexity

The improbabilities of separation distances and slip-vector consistency may be combined to form a more complete probability measure based on rupture complexity. It would be computed pairwise among subsections, with both terms applied in the probability product. This approach could be applied as *a priori* rupture weighting or as part of an a *posteriori* evaluation strategy.

References Cited

Aochi, H., Madariaga, R., and Fukuyama, E., 2002, Effect of normal stress during rupture propagation along non-planar faults: Journal of Geophysical Research, v. 107, no. B2, p. 2038, doi:10.1029/2001JB000500.

Bouchon, M., Campillo, M., and Cotton, F., 1998, Stress field associated with the rupture of the 1992 Landers, California, earthquake and its implications concerning the fault strength at the onset of the earthquake: Journal of Geophysical Research, v. 103, p. 21091–21097, doi:10.1029/98JB01982.

Bouchon, M., and Streiff, D., 1997, Propagation of a shear crack on a nonplanar fault—A method of calculation: Bulletin of the Seismological Society of America, v. 87, p. 61–66.

Duan, B., and Oglesby, D.D., 2006, Heterogeneous fault stress from previous earthquakes and the effect of dynamics of parallel strike-slip faults: Journal of Geophysical Research, v. 111, no. B05309, doi:10.1029/2005JB004138.

Field, E.H., Dawson, T.E., Felzer, K.R., Frankel, A.D., Gupta, V., Jordan, T.H., Parsons, T., Peterson, M.D., Stein, R.S., Weldon, R.J., and Wills, C.J., 2009, Uniform California earthquake rupture forecast—version 2 (UCERF2): Bulletin of the Seismological Society of America, v. 99, p. 2053–2107.

Harris, R.A., Archuleta, R.J., and Day, S.M., 1991, Fault steps and the dynamic rupture process—2-d numerical simulations of a spontaneously propagating shear fracture: Geophysical Research Letters, v. 18, p. 893–896.

Harris, R.A., and Day, S.M., 1999, Dynamic 3-D simulations of earthquakes on en echelon faults: Geophysical Research Letters, v. 26, p. 2089–2092.

Harris, R.A., Dolan, J.F., Hartleb, R., and Day, S.M., 2002, The 1999 Izmit, Turkey, earthquake—A 3D dynamic stress transfer model of intra-earthquake triggering: Bulletin of the Seismological Society of America, v. 92, p. 245–255.

Kame, N., Rice, J.R., and Dmowska, R., 2003, Effect of prestress state and rupture velocity on dynamic fault branching: Journal of Geophysical Research, v. 108, p. 2265, doi:10.1029/2002JB002189.

Kase, Y., and Day, S.M., 2006, Spontaneous rupture processes on a bending fault: Geophysical Research Letters, v. 33, no. L10302, doi:10.1029/2006GL025870.

King, G.C.P., Stein, R.S., and Lin, J., 1994, Static stress changes and the triggering of earthquakes: Bulletin of the Seismological Society of America, v. 84, p. 935–953.

Lin, J., and Stein, R.S., 2004, Stress triggering in thrust and subduction earthquakes, and stress interaction between the southern San Andreas and nearby thrust and strike-slip faults: Journal of Geophysical Research, v. 109, no. B02303, doi:10.1029/2003JB002607.

Lozos, J.Z., Oglesby, D.D., Duan, B., Wesnousky, S.G., 2011, The effects of double fault bends on rupture: Bulletin of the Seismological Society of America, v. 101, p. 385–398.

Oglesby, D.D., 2005, The dynamics of strike-slip step-overs with linking dip-slip faults: Bulletin of the Seismological Society of America, v. 95, p. 1604–1622.

Oglesby, D., 2008, Rupture termination and jump on parallel offset faults: Bulletin of the Seismological Society of America, v. 98, p. 440–447.

Parsons, T., Field, E.H., Page, M.T., and Milner, K., 2012, Possible earthquake rupture connections on mapped California faults ranked by calculated Coulomb linking stresses: Bulletin of the Seismological Society of America, v. 102, p. 2667–2676, doi:10.1785/0120110349.

Parsons, T., Stein, R.S., Simpson, R.W., and Reasenberg, P.A., 1999, Stress sensitivity of fault seismicity—A comparison between limited-offset oblique and major strike-slip faults: Journal of Geophysical Research, v. 104, p. 20183–20202.

Poliakov, A.N.B., Dmowska, R., and Rice, J.R., 2002, Dynamic shear rupture interactions with fault bends and off-axis secondary faulting: Journal of Geophysical Research, Solid Earth, v. 107, no. B11, p. 2295, doi:10.1029/2001JB000572.

Reasenberg, P.A., and Simpson, R.W., 1992, Response of regional seismicity to the static stress change produced by the Loma Prieta earthquake: Science, v. 255, p. 1687–1690.

Shaw, B.E., and Dieterich, J.H., 2007, Probabilities for jumping fault segment stepovers: Geophysical Research Letters, v. 34, no. L01307, doi:10.1029/2006GL027980.

Toda, S., Stein, R.S., Sevilgen, V., and Lin, J., 2011, Coulomb 3.3 graphic-rich deformation and stress-change software for earthquake, tectonic, and volcano research and teaching—User guide: U.S. Geological Survey Open-File Report 2011-1060, 66 p., available at *http://pubs.usgs.gov/of/2011/1060/*.

Wesnousky, S.G., 2006, Predicting the endpoints of earthquake ruptures: Nature, v. 444, p. 358–360.

Wesnousky, S.G., 2008, Displacement and geometrical characteristics of earthquake surface ruptures—Issues and implications for seismic-hazard analysis and the process of earthquake rupture: Bulletin of the Seismological Society of America, v. 98, p. 1609–1632.

Wesnousky, S.G., and Biasi, G.P., 2011, The length to which an earthquake will go to rupture: Bulletin of the Seismological Society of America, v. 101, p. 1948–1950.